Journal of Trace Elements in Medicine and Biology xxx (xxxx) xxx–xxx

Contents lists available at ScienceDirect

Journal of Trace Elements in Medicine and Biology

journal homepage: www.elsevier.com/locate/jtemb

Salicylamide derivatives for iron and aluminium sequestration. From synthesis to complexation studies

Joanna I. Lachowicz[a,*], Miriam Crespo-Alonso[a], Claudia Caltagirone[a], Giancarla Alberti[b], Raffaela Biesuz[b], James O. Orton[c], Valeria M. Nurchi[a]

[a] Dipartimento di Scienze Chimiche e Geologiche, Università di Cagliari, Cittadella Universitaria, I-09042 Monserrato-Cagliari, Italy
[b] Dipartimento di Chimica, University of Pavia, Pavia, Italy
[c] Faculty of Natural and Environmental Sciences, University of Southampton, Southampton, United Kingdom

ARTICLE INFO

Keywords:
Chelating agents
Iron toxicity
Aluminium toxicity
Metal complex stability
Potentiometry
UV-Vis spectrophotometry

ABSTRACT

This paper presents an easy, fast and economic synthesis of chelating agents for medical, environmental and analytical applications, and the evaluation of the stability of their complexes with Fe^{3+} and Al^{3+}. Complex formation equilibria with Cu^{2+} and Zn^{2+} metal ions were also studied to evaluate if the chelating agents can perturb the homeostatic equilibria of these essential metal ions. Effective chelating agents for metal ions, in addition to their well-known medical uses, find an increasing number of applications in environmental remediation, agricultural applications (supplying essential elements in an easily available form), and in analytical chemistry as colorimetric reagents. Besides the stability of the complexes, the lack of toxicity and the low cost are the basic requisites of metal chelating agents. With these aims in mind, we utilized ethyl salicylate, a cheap molecule without toxic effects, and adopted a simple synthetic strategy to join two salicylate units through linear diamines of variable length. Actually, the mutual position of the metal binding oxygen groups, as well as the linker length, affected protonation and complex formation equilibria. A thorough study of the ligands is presented. In particular, the complex formation equilibria of the three ligands toward Fe^{3+}, Al^{3+}, Zn^{2+} and Cu^{2+} ions were investigated by combined potentiometric and spectrophotometric techniques. The results are encouraging: all the three ligands form stable complexes with all the investigated metal ions, involving the oxygen donor atoms from the 2-hydroxybenzamido unit, and nitrogen atoms in copper and zinc coordination.

1. Introduction

Metal ion toxicity is nowadays a primary topic in medicinal, environmental and agricultural chemistry, and the research of new metal chelators is still a leading motif in scientific studies.

Iron chelation therapy entered in clinical practice in the seventies of last century to contrast the toxic effects of iron overload in transfused β-thalassemia patients. Desferal, (N′-{5-[acetyl(hydroxy)amino]pentyl}-N-[5-({4-[(5-aminopentyl)(hydroxy)amino]-4-oxobutanoyl}amino) pentyl]-N-hydroxysuccinamide), the first iron chelator for the treatment of iron overload, has radically changed life expectancy and quality of life of patients. However, it presents several drawbacks, the main ones being its high cost, the lack of oral activity, and the low compliance of patients [1,2].

The joined efforts of biomedical and chemical researchers led, in the first years of this century, to the introduction of two oral chelating agents, deferiprone and deferasirox, which simplified the drug administration and made the treatment more accessible. Still, they present a number of deleterious side effect [3–5]. Therefore, the research for cheap, effective, and safe iron chelators constitutes an obligatory necessity [6]. For similar reasons the research on chelators for copper overload (Wilson's disease) is always compelling [7].

Further, any chelating agent must be selective toward iron. This implies that the stability of iron chelates has to be considerably higher than that of the complexes with essential metal ions, which must not perturb iron chelation. Therefore, a full characterization of the behaviour in biological fluids of any chelating agents intended for iron chelation is mandatory, and the study of the complex formation equilibria with essential copper and zinc metal ions is always recommended.

Metal chelating agents, in addition to their well-known clinical uses, find an increasing amount of applications in environmental remediation [8–10] and in agriculture for delivering essential elements in an easily accessible form, or making available the elements existing in the soil

* Corresponding author.
E-mail address: lachowicz@unica.it (J.I. Lachowicz).

https://doi.org/10.1016/j.jtemb.2018.04.010
Received 15 January 2018; Received in revised form 14 March 2018; Accepted 10 April 2018

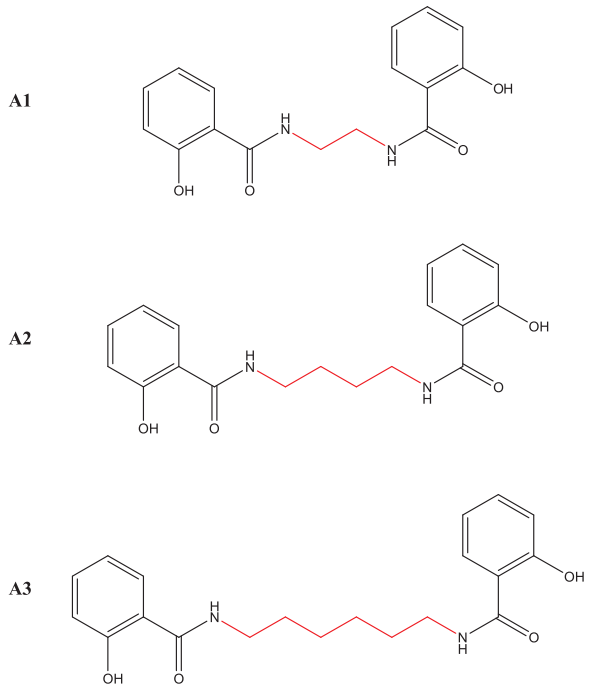

Scheme 1. Molecular structures of 1,2-bis(2-hydroxybenzamido) ethane (A1), 1,4-bis(2-hydroxybenzamido) butane (A2) and 1,6-bis(2-hydroxybenzamido) hexane (A3) ligands.

[11–13]. The fundamental requisites of metal chelators for these uses are the formation of stable complexes, the absence of toxicity, the biodegradability and the low cost.

With these aims in mind, we synthesized three iron and aluminium chelators reported in Scheme 1.

A simple strategy for the synthesis is proposed: ethyl salicylate, an economic molecule without toxic effects, was used as the basic unit for the new chelators, and a fast synthesis was adopted for joining two 2-hydroxybenzamido units through simple linear diamines of variable length. The simplicity of synthesis allows an easy and low cost preparation. The mutual position of the binding oxygen groups, related to the anchoring position of the linker, as well as the linker length, can affect both the protonation and complex formation equilibria. The thorough study of the ligands, has different aims to asses, in particular:

1 The effectiveness of the simple and economic synthetic method;
2 How the length of the linker affects the protonation constants;
3 The involvement of the nitrogen atoms (in the linker) in the coordination to Cu^{2+} and Zn^{2+} ions;
4 How the structural disposition of these tetradentate ligands favours, as observed previously for a number of kojic acid derivatives [14–22], the formation of binuclear complexes of higher stability than that of salicylamide.

The complex formation and coordination mode of 1,2-bis(2-hydroxybenzamido) ethane (A1), 1,4-bis(2-hydroxybenzamido) butane (A2) and 1,6-bis(2-hydroxybenzamido) hexane (A3) ligands (Scheme 1) toward Fe^{3+}, Al^{3+}, Zn^{2+} and Cu^{2+} ions has been studied, by combined potentiometric and spectroscopic techniques, and compared with crystal structures and our previous data.

2. Experimental

2.1. Reagents

HCl, NaCl, NaOH, ethyl salicylate, ethyl acetate, toluene, $FeCl_3$, $AlCl_3$, $ZnCl_2$, $CuCl_2$, ethylene diamine, butane-1,4-diamine, and hexane-1,6-diamine were Aldrich products. Carbonate free sodium hydroxide solutions were prepared according to Albert and Serjeant [23].

The metal ion standard solutions were prepared by dissolving the required amount of chloride salts in pure double distilled water and adding a stoichiometric amount of HCl to prevent hydrolysis. Fe^{3+} solution was standardized by spectrophotometric analysis of the Fe^{3+}–desferal complex [24], while Al^{3+}, Cu^{2+} and Zn^{2+} solutions were standardized by EDTA titration.

2.2. General procedure for the synthesis of ligands A1-A3

Ligands **A1-A3** were synthetized as follow: To a stirred solution of ethyl salicylate (2 g, 0.014 mol) in dry toluene (20 mL), diamine (0.007 mol) was added dropwise under argon at room temperature. he resulting solution was warmed up to reflux and stirred for 16 h. After this time, the solvent was removed under reduced pressure and ethyl acetate was added. The resulting suspension was stirred for 2 h and filtered. Ethyl acetate was evaporated and the resulting crude product was purified by flash chromatography (eluents hexanes:diethyl ether 95:5 to 50:50) affording the corresponding pure ligands.

Ligand **A1**, 68% yield. yellow solid, Mp = 179–181 °C, HRMS (ESI): calc. for $C_{16}H_{17}N_2O_4$: 301.1188 ($M+H^+$), found: 301.1191. ^{1}H NMR (400 MHz, DMSO-d_6) δ: 8.56 (br.s, 1 H), 7.39 (d, J = 7.7 Hz, 1 H), 6.81 (t, J = 7.5 Hz, 1 H), 6.38 – 6.21 (m, 2 H), 2.98 (d, J = 4.7 Hz, 2 H), 2.42 (t, J = 6.0 Hz, 2 H), 1.91 (br. s, 1 H); ^{13}C NMR (101 MHz, DMSO-d_6) δ: 169.5, 169.4, 159.9, 133.8, 128.3, 118.6, 117.3, 115.2, 36.5.

Ligand **A2**, 68% yield. yellow solid; Mp = 162–165 °C; HRMS (ESI): calc. for $C_{18}H_{21}N_2O_4$: 329.1501 ($M+H^+$), found: 329.1511. ^{1}H NMR (500 MHz, CD_3OD) δ: 7.81 (dd, J = 7.5, 1.5 Hz, 2 H), 7.28 – 7.25 (m, 2 H), 6.76 (dd, J = 8.0, 12.5 Hz, 2 H), 3.31 (s, 2 H), 2.97(t, J = 7.5 Hz, 2 H), 1.75 (m, 2 H); ^{13}C NMR (126 MHz, CD_3OD) δ: 167.7, 139.0, 133.7, 124.1, 122.3, 109.9, 45.2, 30.8.

Ligand **A3**, 48% yield. yellow solid; Mp = 145–148 °C; HRMS (ESI): calc. for $C_{20}H_{25}N_2O_4$: 357.1814 ($M+H^+$), found: 357.1817. ^{1}H NMR (500 MHz, CD_3OD) δ: 7.84 (t, J = 9.5, 1.0 Hz, 2 H), 7.30 – 7.25 (m, 2 H), 6.68 (dd, J = 9,5, 16.5 4 H), 2.89 (t, J = 9.5 Hz, 2 H), 1.63 – 1.62 (m, 2 H), 1.39-1.35 (m, 2 H); ^{13}C NMR (126 MHz, CD_3OD) δ: 176.3, 162.5, 134.0, 131.6, 128.9, 119.1, 117.2, 40.5, 28.3, 26.9.

High Resolution Mass Spectra (HRMS) were obtained using a Bruker High Resolution Mass Spectrometer in fast atom bombardment (FAB+) ionization mode or acquired using an Bruker micrOTOF-Q II 10027. Melting points were determined with a Büchi M-560. Analytical thin layer chromatography was performed using 0.25 mm Aldrich silica gel 60-F plates. Flash chromatography was performed using Merk 70–200 mesh silica gel. Yields refer to chromatography and spectroscopically pure materials.

2.3. Potentiometric-spectrophotometric measurements

Protonation and complex formation equilibria were studied in a thermostatted glass cell, equipped with a magnetic stirrer, a Metrohm LL UNITRODE glass combined electrode connected to a Metrohm 691 pH-meter, a microburet delivery tube connected to a Dosimat 665 Metrohm titrator, an inlet–outlet tube for Argon and a fiber optic dip probe connected to a Varian Cary 50 UV–vis spectrophotometer. The electrode was calibrated daily in hydrogen ion concentration as previously described [15]. The calculations were performed with Hyperquad2013 [25] and HypSpec2014 [26] programs. The protonation equilibria were studied at ligand concentration 5×10^{-4} M and the complex formation equilibria at a constant ligand concentration 5×10^{-4} M and 1:1, 1:2 and 1:3 metal/ligand molar ratios, ionic strength 0.1 M (NaCl). The samples were titrated with 0.1 M NaOH at 25.0 °C in the pH range 2–11. Protonation and Cu^{2+} and Fe^{3+} complex formation equilibria were studied using a previously described combined spectrophotometric-potentiometric procedure [21], while Al^{3+}

and Zn^{2+} complex formation equilibria were studied only by potentiometry. Standard deviations computed by Hyperquad and HypSpec refer to random errors only. They are, however, a good indication of the importance of the particular species involved in the equilibrium. Log β_{pqr} values refer to the overall equilibria $pM + qH + rL \leftrightarrows M_pH_qL_r$ (electrical charges omitted), and L represents the completely deprotonated ligand.

2.4. Diffractometry

In a tentative of preparing solid state complexes between Cu^{2+} and the longer ligands A2 and A3 we obtained (from a water solution, equimolar in A2 and copper chloride and acid by HCl addition), a crystal of the "complex" between copper and dba (the linker of the ligand) of $CuCl_4^{2-} \times [C_4H_{14}N_2]^{2+}$ composition. A small portion of this sample was suspended in perfluoroether oil; a suitable single clear dark green irregular block-shaped crystal of size (0.15 × 0.08 × 0.04) mm^3 was selected and mounted on a MITIGEN holder. This crystal was then aligned upon a Rigaku AFC12 FRE-VHF diffractometer. The crystal was kept at $T = 100(2)$ K during data collection. Using Olex2 [27], the structure was solved with the ShelXT [28] structure solution program, using the Intrinsic Phasing solution method. The model was refined with version 2014/7 of ShelXL [29] using Least Squares minimisation.

3. Results and discussion

3.1. Protonation equilibria

Protonation constants of the three A1-A3 ligands were determined by potentiometric and spectrophotometric methods. These ligands are characterized by three protonation equilibria, two relative to the phenolate groups and the remaining one relative to the protonation of one amide nitrogen atom. The values of the protonation constants for the three ligands, evaluated from potentiometric data using the HyperQuad program [25] are reported in Table 1. A fourth protonation step was not observed for the three ligands.

The first two equilibria were studied by joined potentiometric-spectrophotometric titrations of 5×10^{-4} M ligand solutions with NaOH 0.1 M. The UV spectra were collected after each addition of base. As an example, selected spectra of ligand A1collected during the titration are shown in Fig. 1, and the speciation plot for this ligand is reported in Scheme S1,

The spectra collected during UV titration, though not relevant for protonation constant calculation, allow attributing the first two protonations to the two phenolate groups. In fact, the protonation of a phenolate groups is accompanied by strong spectral variations in the 250–400 nm spectral range [14–22] (Fig. 1), while the protonation of an amide group is practically spectrophotometrically silent. The band at 347 nm present in basic environment (pH 10.76) progressively transforms in one centered at 300 nm as pH decreases to 9, with a clear isosbestic point at 318 nm. From pH 8 to pH 5 a further decrease of the band at 347 nm is observed, with a contemporary increase of the 300 nm band. In this second protonation step, a small shift of the isosbestic point to higher wavelengths is observed. No further spectral variations take place in the third protonation step. Based on the above

Table 1
Protonation constants (log K) of A1, A2 and A3 ligands at 25 °C and 0.1 M NaCl ionic strength.

Species	A1 log K	A2 log K	A3 log K
$[LH]^-$	10.73(2)	11.91(4)	11.71(3)
LH_2	6.64(2)	9.60(3)	10.12(2)
$[LH_3]^+$	1.96(4)	3.22(1)	3.37(1)

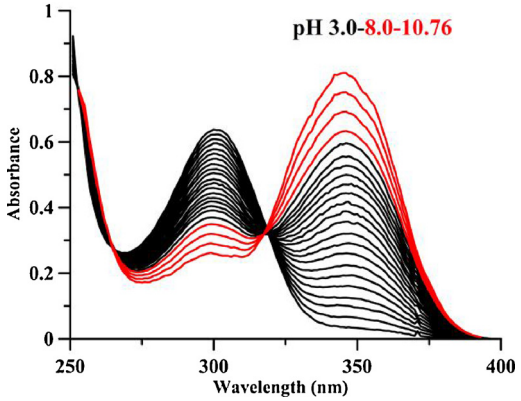

Fig. 1. Selected spectra collected during the base titration of A1 ligand, 1×10^{-3} M, path length 0.2 cm.

observations the first two steps of protonation can be univocally attributed to the phenolate groups and the third to the amide nitrogen atom. The analysis of the results in Table 1 shows that the log K1 for the three ligands ranges from 10.73 for A1 to 11.91 for A2, in any case 2–3 units higher than that of a free phenolate [30]. This can be explained by the formation of stabilizing hydrogen bonds between the phenolic group and the carbonilic unit of the proximal amido group, as shown by the crystal structure of the A1 ligand in Fig. 2 (blue dotted line). The second point to be remarked is, besides the general lowering of the second protonation constant dependent on the chain length, the impressive lowering of the second protonation constant of A1. A similar trend is presented also by the log K values of the protonation of nitrogen atoms in the constituting amines (Table 2). This can be explained in some amount by the possible intermolecular hydrogen bonds between the phenolic groups in one molecule and the nitrogen atoms in the second (Fig. 2, red dotted line), as shown in the crystal structure presented by da Costa et al. [31].

Presumably, a similar scheme of hydrogen bonding becomes even more difficult for longer chain lengths of A2 and A3 ligands.

The third protonation relative to a nitrogen atom (in the linker) is characterized by values ranging from 1.96 in A1 to 3.37 in A3. This trend is similar to that of log K_2 values, and presumably the same intermolecular hydrogen bonds account also for the log K_3 values. The protonation constants of the nitrogen atoms in the amide groups of A1-A3 ligands are quite different from those for the corresponding amines

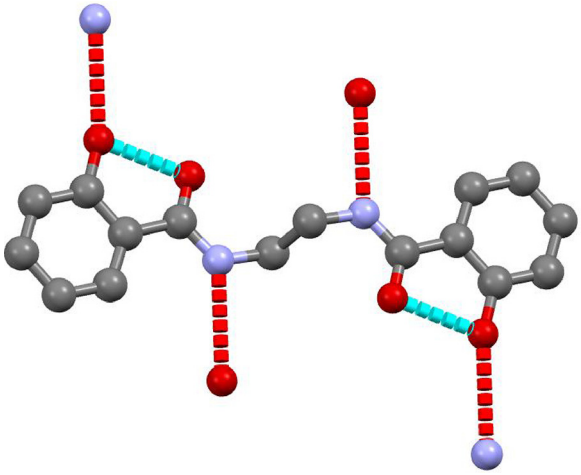

Fig. 2. Crystal structure of the ligand A1 [31] (O—red; N—blue, C—grey). Coordinates obtained from the CambridgeStructural Database, image created with Mercury3.5. (For interpretation of the references to colour in this figure legend, the reader is referred to the web version of this article).

Table 2
Protonation constants (log K) of ethylene diamine (en), butane-1,4-diamine (dba), and hexane-1,6- diamine (dha), used as linkers in A1, A2, A3 respectively, at 25 °C and 0.1 M NaCl ionic strength.

Species	en	dba	dha
$[LH]^{+}$	9.81(4)	10.85(4)	10.94(4)
$[LH_2]^{2+}$	7.08(3)	9.70(2)	10.05(3)

Literature comparison values: (**en**) 9.94, 7.10 [32], 9.84, 7.06 [33]; (**dba**) 10.58, 9.32 [32], 10.57, 9.31 [34]; (**dha**) 10.94, 10.05 [32], 10.93, 10.05 [34].

shown in Table 2. In fact, compared to amines, amides are weaker bases. Therefore, amides do not present noticeable acid–base properties in water. The low basicity of amides can be explained by the electron-withdrawing properties of the carbonyl group versus the lone pair of electrons on the nitrogen. Nonetheless, thanks to the presence of N—H dipoles the amides can act also as H-bond donors, and can participate in hydrogen bonding with water enhancing water solubility of amides.

3.2. Iron complexes

The complex formation equilibria of all three ligands with Fe^{3+} ions were studied by combined potentiometric–spectrophotometric techniques. In fact, being iron almost completely complexed when mixing reagents before the potentiometric titrations with base, reliable complex formation constants could be not estimated from potentiometric data alone. Therefore, the complex formation equilibria were studied both on sets of solutions at increasing concentrations of HCl until the disappearance of the bands of complexed iron in the pH range 0–2, (Fig. 3A) and by base titration in the pH range 2–5 (Fig. 3B).

The spectra in Fig. 3A, collected in high acidic solutions, show the formation of one unique species from pH 0 to pH 2. The position of the band (527 nm) and its absorptivity value, with respect to iron, ($\varepsilon = 716\ M^{-1}\ cm^{-1}$) are very similar to the values found for the 1:1 Fe^{3+}-salicylic acid complex (525 nm, $\varepsilon = 630\ M^{-1}\ cm^{-1}$) [30]. This is consistent with the formation of a complex $[Fe_2LH]^{5+}$, in which the ligand A1 binds two iron ions through the phenolate and the amido carbonyl groups of each salicyl amide unit, being one of the nitrogen atoms in the linker till protonated. The further increase of pH during the basic titration (Fig. 3B) causes the progressive formation of a new band centered at 478 nm, with an increase of absorptivity. These spectral variations are similar to those observed for the formation of the FeL_2 complex of iron with salicylic acid [30]. In the case of ligand A1, which cannot bind one iron ion with both the salicyl amide units for steric reasons, a conceivable model is the formation of a $[Fe_2L_2]$ complex in which each iron ion is coordinated via the oxygen atoms of two amide moieties, one from each ligand, as visible in Fig. 4A, which presents the solid state structure of the complex $Fe_2(A1)_2$ (crystals from water) [35] and in Fig. 4 B (crystals from methanol) [36].

In Fig. 4C the analogous complexes of iron with ligand A2 are reported [36].

In our case the two iron atoms are joined by two molecules of μ-water that can lose protons giving the neutral $Fe_2L_2H_{-2}$ complex. The complexation models for the three ligands with Fe^{3+} and the associated stability constants evaluated with HypSpec [26] and Hyperquad [25] programs are reported in Table 3. This Table reports also the pK values related to the different deprotonation steps of the complexes. In the case of ligand A2 and A3 the first pK is easily attributed to the deprotonation of the amide group, being the value almost identical to that of the free ligand, and the successive pK's

The constants for the Fe^{3+} hydroxides at 25 °C and 0.1 M ionic strength, taken from Baes and Mesmer [37], were considered in Hyperquad and Hyss calculations. *Negative logarithm of the concentration of the free metal in solution, calculated for total [ligand] = 10^{-5}M and total [metal] = 10^{-6}M at pH 7.4.

to the loss of protons from the coordinated μ-water molecules. In the case of ligand A1 the protons of the amide group and the first from coordinated water are lost together, presumably the shorter linker favoring the formation of stabilizing hydrogen bonds.

The related speciation plots are shown in Fig. 5. Despite the higher complex formation constants

with A2 and A3, the pFe values are almost similar, and this depends on the lower value of protonation constants of A1. The calculated pFe values can be compared with the corresponding value for the complexes between Fe^{3+} and the salicylamide, that forms FeL and FeL_2 complexes [38]. Salicylamide is characterized by a protonation constants 8.89 at 25 °C and $NaClO_4$ 3 M ionic strength, and by the Fe^{3+} complex formation constants log β_{11} 10.02 and log β_{12} 16.26 in the same experimental conditions; from these values a pFe 9.62 can be calculated. The presence of two linked salicylamide units in the A1-A3 ligands leads to the significant increase of the stability of complexes compared with that of salicylamide, in particular the pFe value 9.62 for salicylamide increases of 4.1units passing to A1, and of 4.4 units passing to A3. As reported previously [39], this fact remarks that, if the linker has the correct length and flexibility to allow the best iron coordination without strain, the enthalpic contribution to the formation complexes should be similar to that of salicylamide, which is not disturbed by strain effects. Consequently, the entropic contribute which depends on

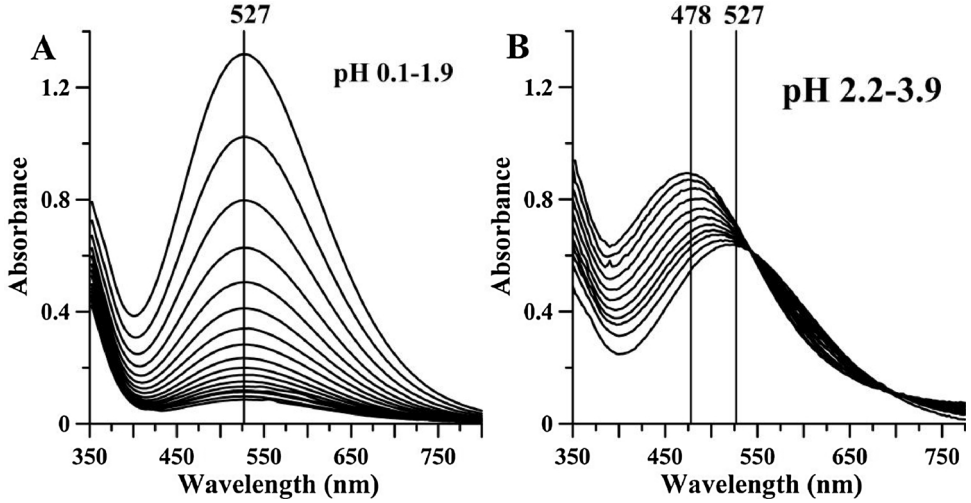

Fig. 3. A) Selected spectra of the system A1-Fe^{3+} collected between pH 0.1 and pH 1.9; $[Fe^{3+}] = 2.07 \times 10^{-3}$ M, [A1] = 4.12×10^{-3} M, path length 1 cm; B) selected spectra of the system A1-Fe^{3+} collected between pH 2.2 and pH 3.9; $[Fe^{3+}] = 9.93 \times 10^{-4}$ M, [A1] = 2.01×10^{-3} M, path length 1 cm.

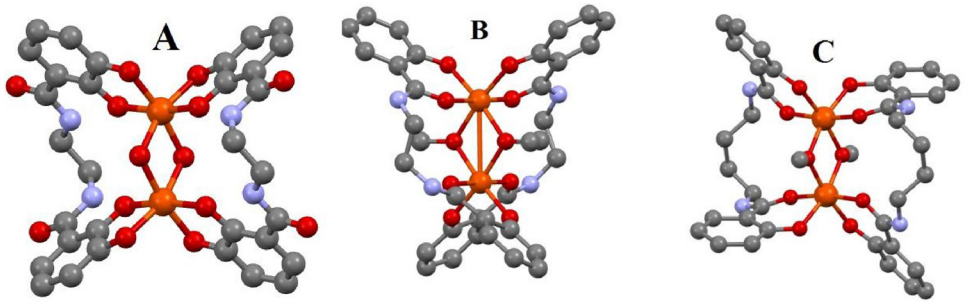

Fig. 4. A) Crystal structure of the complex between two Fe^{3+} ions and two A1 ligands in water [35], B) methanol [36] and C) crystal structure of the complex between two Fe^{3+} ions and two A2 ligands [36] (Fe—orange; O—red; N—blue, C—grey). Coordinates obtained from the Cambridge Structural Database, images created with Mercury 3.5. (For interpretation of the references to colour in this figure legend, the reader is referred to the web version of this article).

Table 3
Complex formation constants (logβ and pK) of A1, A2 and A3 ligands with Fe^{3+} at 25 °C and 0.1 M NaCl ionic strength.

Species	A1		A2		A3	
	log β	pK	log β	pK	log β	pK
$[Fe_2LH]^{5+}$	22.96(2)		27.16(4)		26.92(3)	
$[Fe_2L_2H]^{3+}$	38.48(5)		45.64(3)		46.20(4)	
$[Fe_2L_2]^{2+}$		4.64	42.41(3)	3.23	42.81(4)	3.39
$[Fe_2L_2H_{-1}]^{+}$	29.20(6)	4.64	36.44(4)	5.97	37.12(3)	5.69
$Fe_2L_2H_{-2}$	23.2(1)	6.0	30.30(5)	6.14	31.02(4)	6.10
pFe*	13.71		13.95		14.00	

Table 4
Complex formation constants (logβ and log K) of A1, A2 and A3 ligands with Al^{3+} at 25 °C and 0.1 M NaCl ionic strength.

Species	A1		A2		A3	
	log β	log K	log β	log K	log β	log K
$[Al_2LH]^{5+}$	19.85(5)		24.22(3)		25.28(4)	
$[Al_2L_2]^{2+}$	28.85(3)		37.50(4)		40.61(4)	
$[Al_2L_2H_{-1}]^{+}$	22.83(3)	6.02	31.48(3)	6.12	34.46(2)	6.15
$Al_2L_2H_{-2}$	16.62(4)	6.21	25.18(2)	6.30	28.10(3)	6.36
pAl*	10.42		11.40		12.86	

The constants for the Al^{3+} hydroxides at 25 °C and 0.1 M ionic strength, taken from Baes and Mesmer [37] were considered in Hyperquad and Hyss calculations. * Negative logarithm of the concentration of the free metal in solution, calculated for total [ligand] = 10^{-5}M and total [metal] = 10^{-6}M at pH 7.4.

the preorganization of the tetradentate ligand, strongly favors the formation of the Fe_2L_2 complexes observed for A1-A3 ligands, and leads to increase of pFe.

3.3. Aluminium complexes

Due to the lower stability of the complexes formed with aluminium than that of those formed with iron, the complex formation equilibria were reliably studied by potentiometric measurements. The complexation scheme, as expected, strictly resembled that observed with iron. The complex formation constants are reported in Table 4 and the related speciation plots in Figs. 6.

As a first observation, the increasing stability of aluminium complexes with the length of the linker has to be remarked. This determines that, while the complexes with A1 are stable till pH8, when they decompose giving the free ligand and $Al(OH)_4^-$, those with A2 are stable till pH 9 and those with A3 till pH 10. A second consideration is based on the ratios pAl/pFe, which are an inverse measure of the selectivity of ligands for iron. This ratios range between 0.6 and 0.7, for a high number of ligands (in particular oxygen binding ligands). With the present ligands these ratios are 0.76 for A1, 0.81 for A2 and 0.93 for A3, indicative of a particular stabilization of the aluminium complexes presumably related to its lower dimension. As done for iron complexes, we compare the found pAl values with that related to the salicylamide aluminium complexes. On the basis of the unique literature value found for this system [40] a pAl 7.14 was calculated, so an increases of 3.3 units can be calculated passing to A1, 4.2 passing to A2 and 5.7 units passing to A3. The same considerations on the entropic contribute made for iron are valid. In particular the outstanding increase in stability passing to the ligand A3 has to be remarked, that renders this chelating agent appropriate for further studies for medical applications, even if it is still lower than the pAl 16 for deferiprone [41].

3.4. Copper complexes

The potentiometric data for the complex formation equilibria between the three ligands and Cu^{2+} were fitted assuming only the formation of variously protonated 1:1 complexes (Table 7). This is in line

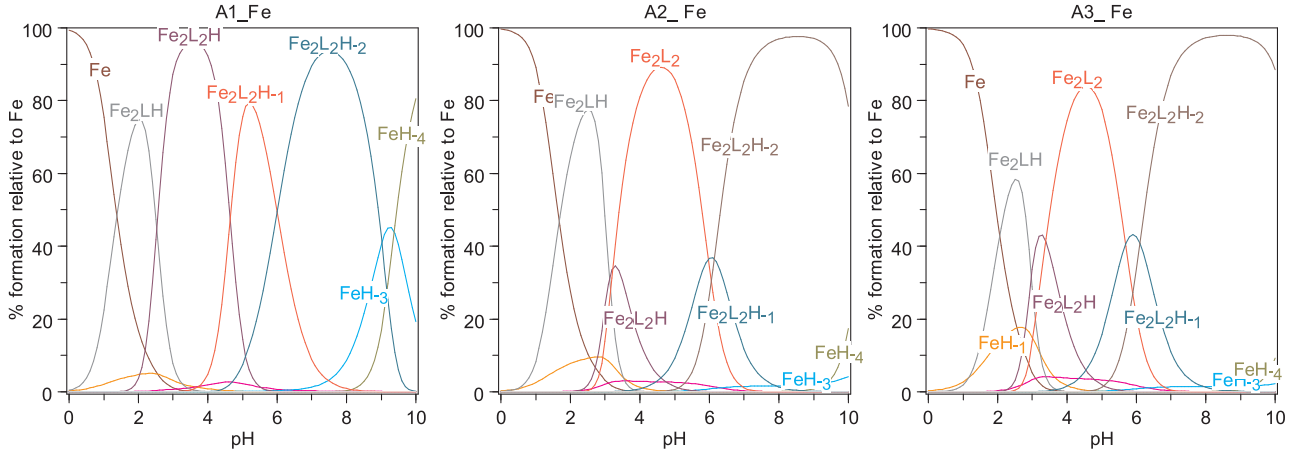

Fig. 5. Speciation plots of the three ligands A1-A3 with Fe^{3+} calculated with the stability constants in Table 3, at Fe^{3+} concentration 1×10^{-3} M and ligand concentration 2×10^{-3} M.

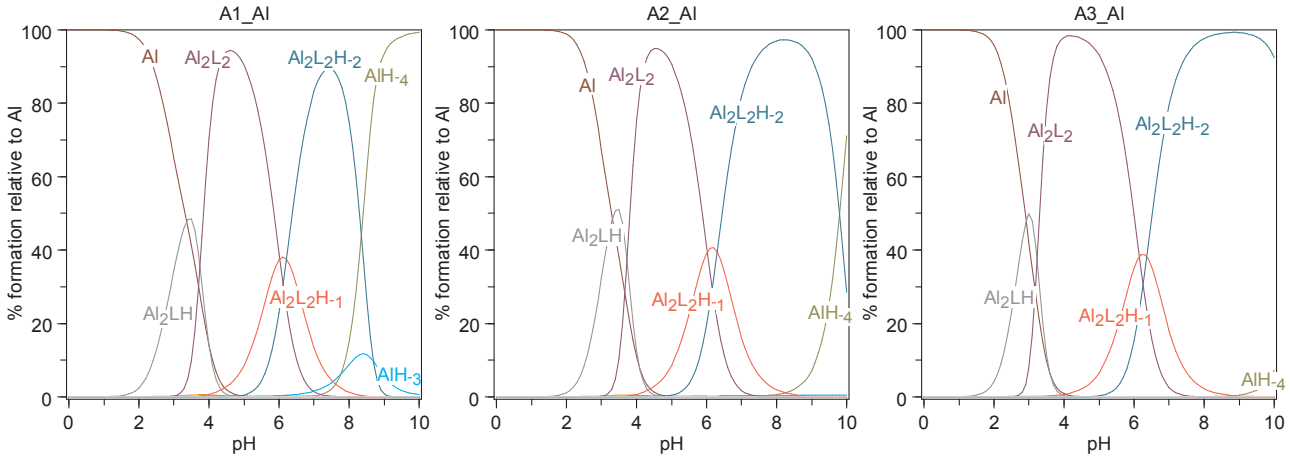

Fig. 6. Speciation plots of the three ligands A1-A3 with Al^{3+} calculated with the stability constants in Table 4, at Al^{3+} concentration 1×10^{-3} M and ligand concentration 2×10^{-3} M.

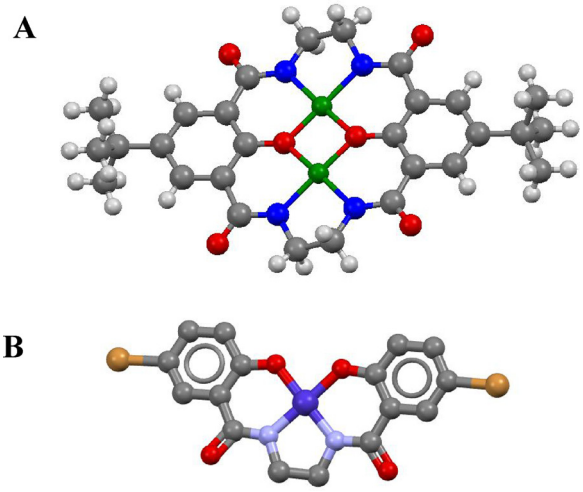

Fig. 7. A) Crystal structure of the complex between two Cu^{2+} ions and the cyclic ligand bis(tetra-N-butylammonium)-(10,21-di-t-butyl-23,24-bis(hydroxy)-3,6,14,17-tetraazatricyclo[17.3.1.18,12]te tracosa-1(23),8(24),9,11,19,21-hexaene-2,7,13,18-tetronato, containing the A1 unit [42], and B) crystal structure of the complex between Co^{2+} ion and a dibromide derivative of A1 ligand [43] (H-white, Cu—green; Co-violet; Br- brown; O—red; N—blue, C—grey). Coordinates obtained from the Cambridge Structural Database, image created with Mercury 3.5. (For interpretation of the references to colour in this figure legend, the reader is referred to the web version of this article).

with the structures of the copper complex with an analogous ligand (Fig. 7A) and for the Co^{2+} complex with a dibromide derivative of A1 (Fig. 7B).

Differently from Fe^{3+} and Al^{3+} complexes, Cu^{2+} ions are coordinated by the nitrogen atoms in the linker and the phenolate group of the salicylamide unit, while the carbonyl groups are not involved in coordination. The data in Table 5 and the speciation plots in Fig. 9 give evidence of the remarkably higher stability of the complexes with ligand A1. This is in line with the behavior of Cu^{2+} ion with the diamines in the linker (Table S1). In fact, copper forms stable metal complexes with ethylene diamine (en) (pCu 9.9) in solution (Table S1) and solid state [44], and complexes of low stability with the longer butane-1,4-diamine (dba).

Dba forms very low stability copper complexes in water solution [45] and solid state. In a tentative of preparing solid state complexes between Cu^{2+} and the longer ligands A2 and A3, we obtained a crystal of the "complex" between copper and dba, whose structure is shown in

Table 5
Complex formation constants (logβ and log K) of A1, A2 and A3 ligands with Cu^{2+} at 25 °C and 0.1 M NaCl ionic strength.

Species	A1		A2		A3	
	log β	log K	log β	log K	log β	log K
$[CuLH]^+$			18.92(3)		19.24(3)	
CuL	9.97(7)		11.57(4)	7.35	12.34(4)	6.9
$[CuLH_{-1}]^-$	3.27(8)	6.7	2.17(5)	9.40	2.81(5)	9.53
pCu*	8.31		6.36		6.54	

The constants for the Cu^{2+} hydroxides at 25 °C and 0.1 M ionic strength, taken from Baes and Mesmer [37], were considered in Hyperquad and Hyss calculations. * Negative logarithm of the concentration of the free metal in solution, calculated for total [ligand] = 10^{-5}M and total [metal] = 10^{-6}M at pH 7.4.

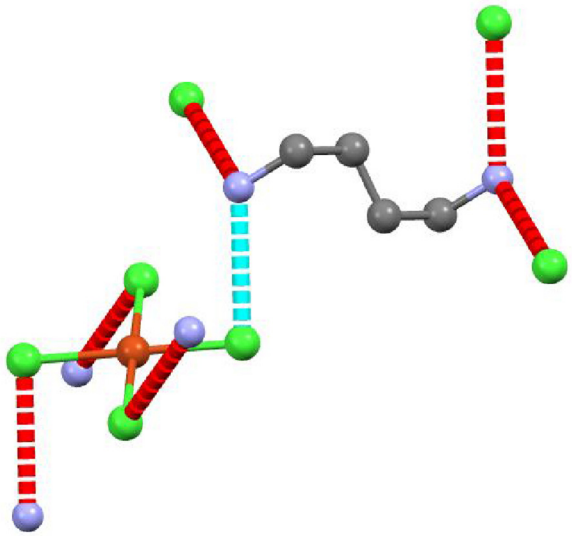

Fig. 8. Crystal structure of the complex between $[CuCl_4]^{2-}$ and dba ligand. (Cu-orange; Cl-green; N- blue; C-grey) (For interpretation of the references to colour in this figure legend, the reader is referred to the web version of this article).

Fig. 8. An alternating organic/inorganic layered structure consisting of discrete square planar $[CuCl_4]^{2-}$ and $[C_4H_{14}N_2]^{2+}$ units, is contacted through a combination of electrostatic and N—HCl hydrogen bonds (2.36 Å, 159.8°). There is close packing within the inorganic layers brings adjacent Cu-ClCu distances just below Van der Waals distance, and the copper centre adopts itself a pseudo octahedral geometry with a

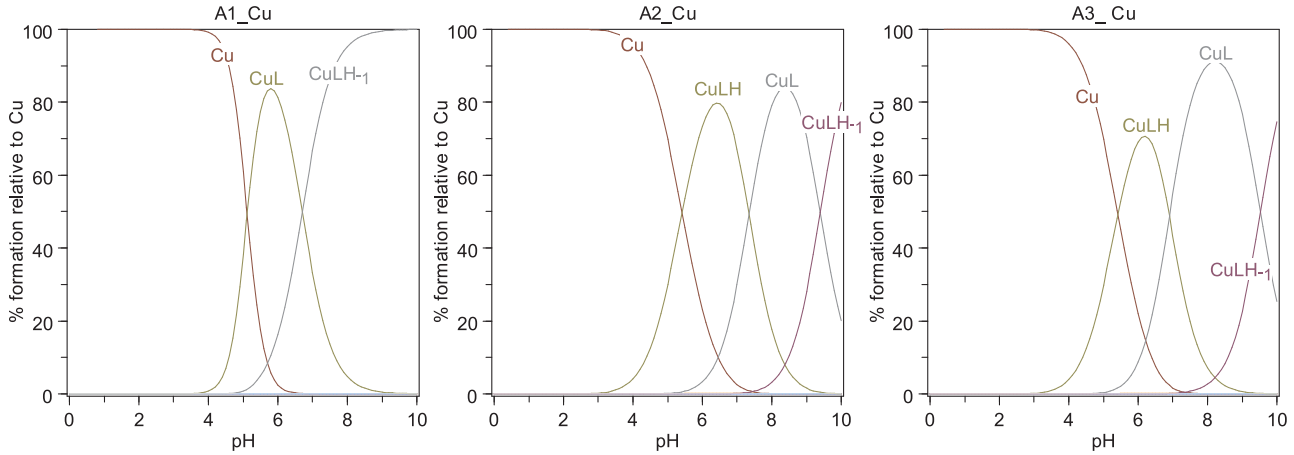

Fig. 9. Speciation plots of the three ligands A1-A3 with Cu^{2+} calculated with the stability constants in Table 5, at Cu^{2+} concentration 1×10^{-3} M and ligand concentration 2×10^{-3} M.

Jahn-Teller distortion; similar to many Copper(II) compounds. In this structure, copper-chlorine short and long distances are 2.38 Å and 3.08 Å respectively. **Crystal Data:** $C_4H_{14}Cl_4CuN_2$, $M_r = 295.51$, monoclinic, $P2_1/c$ (No. 14), a = 9.1857(2) Å, b = 7.5688(2) Å, c = 7.5431(2) Å, $\beta = 103.424(3)^\circ$,$\alpha = \gamma = 90^\circ$, $V = 510.10(2)$ Å^3, $T = 100(2)$ K, $Z = 2$, $Z' = 0.5$, μ(MoKα) = 3.131, 21,510 reflections measured, 1147 unique ($R_{int} = 0.0386$) which were used in all calculations. The final wR_2 was 0.0421 (all data) and R_1 was 0.0168 ($I > 2(I)$). Further information regarding this structure, crystallographic information file, details of data collection and refinement and full crystallographic tables, may be found in the supplementary data.

The copper complexes of A1, A2 and A3 ligands are coloured and were studied with the use of Vis spectrophotometry. As an example, A2 copper complexes spectra are presented in Fig. 10. There is no complex formation at pH below 3 (Fig. 9) and only the bands of free ligand (Fig. 10A, red lines) can be observed. Above pH 3 are forming $[Cu(A2)H]^+$ complexes, which are characterized by the presence of the Vis bands at ~325 (Fig. 10A), ~400 nm (Fig. 10B), assigned as charge transfer O(phenol) → Cu^{2+} transition, and the band at ~700 nm assigned as the N→Cu^{2+} transition. At higher pH, the complexes are transformed in protonless complexes Cu(A2). The dissociation of the last nitrogen atom leads to the appearance of the band ~650 nm (Fig. 10C), attributed to 2N→ Cu^{2+} transition. On the base of UV–vis studies, we can propose the coordination scheme of the copper complex shown in the crystal structure (Fig. 7), where each copper ion is coordinated to pair of O-donor atoms (hydroxyl group) and the pair of N-donor atoms (linker).

3.5. Zinc complexes

The equilibria of the three ligands with zinc ion were studied by potentiometry, and the results are presented in Table 6 and graphically in the speciation plots in Fig. 11. These results resemble those obtained with copper ion, but a lower stability has to be remarked, as expected. Also in this case, ligand A1 forms complexes of particular high stability.

Table 6
Complex formation constants (logβ and log K) of A1, A2 and A3 ligands with Zn^{2+} at 25 °C and 0.1 M NaCl ionic strength.

Species	A1		A2		A3	
	log β	log K	log β	log K	log β	log K
$[ZnLH]^+$	16.21(5)		17.77(3)		17.51(5)	
ZnL	9.61(6)	6.60	10.26(3)	7.51	10.38(3)	7.13
$[ZnLH_{-1}]^-$	2.56(6)	7.05	0.99(5)	9.27	0.45(4)	9.93
pZn*	7.70		6.03		6.02	

The constants for the Zn^{2+} hydroxides at 25 °C and 0.1 M ionic strength, taken from Baes and Mesmer [37], were considered in Hyperquad and Hyss calculations. * Negative logarithm of the concentration of the free metal in solution, calculated for total [ligand] = 10^{-5}M and total [metal] = 10^{-6}M at pH 7.4.

4. Conclusions

The three studied ligands, characterized by a different length of the linker (2, 4 and 6 CH_2 groups between the two amide groups) present a specific behavior for each kind of metal ion. In particular:

- In the case of the trivalent hard metal ions binuclear complexes are formed, and the stability is greater than those formed with the chelating moiety salicylamide alone. This is due to the entropic contribute favored by the preorganization of the tetradentate ligands for the formation of the Fe_2L_2 complexes. The increase of

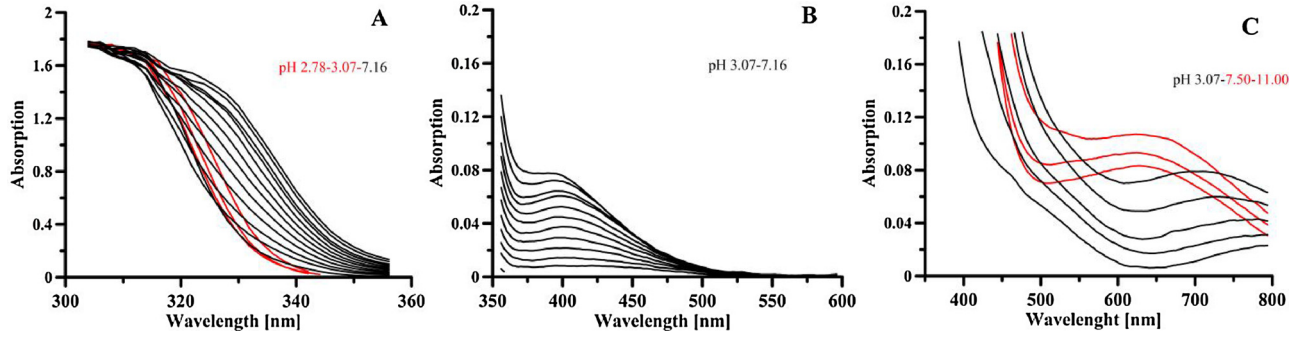

Fig. 10. The Vis spectra of Cu(II)/A2 complex formation in the range A) 300–360 nm, [A2] = 1 mM, 1:1 metal:ligand molar ratio, l = 0.2 cm; B) 350-600 nm, [A2] = 1 mM, 1:1 metal:ligand molar ratio, l = 1 cm; C) 350-800 nm, [A2] = 6.5 mM, 1:1 stoichiometry, l = 1 cm.

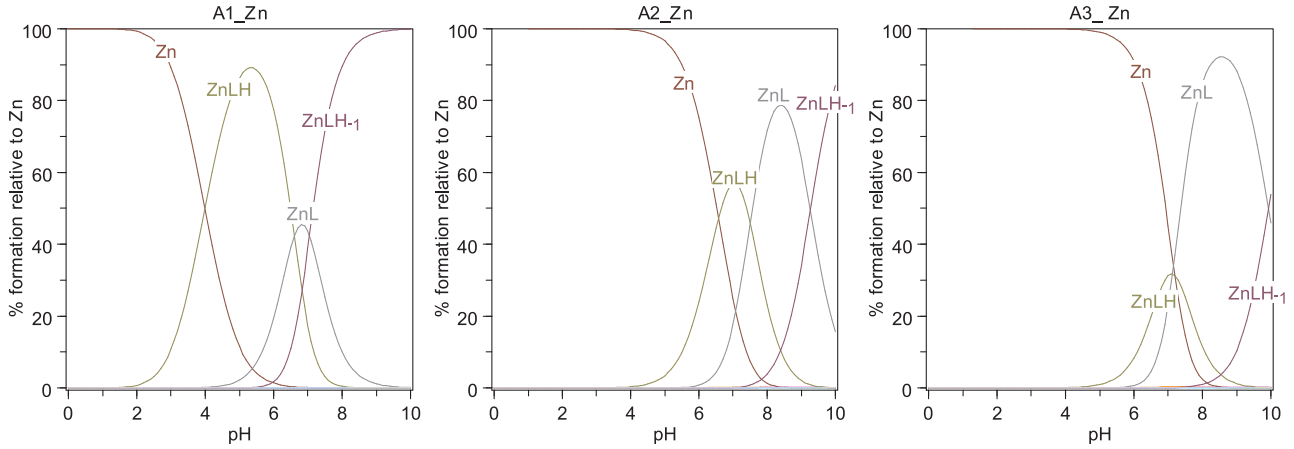

Fig. 11. Speciation plots of the three ligands A1-A3 with Zn^{2+} calculated with the stability constants in Table 6, at Zn^{2+} concentration 1×10^{-3} M and ligand concentration 2×10^{-3} M.

stability, observed with the length of the linker (mainly with aluminium ion), is surely dependent on the greater flexibility offered by the longer linkers. The pFe stability values obtained with the three ligands surely prevent their biomedical application as iron chelating agents, but are indicative for possible uses in bioremediation and in agriculture use. The peculiar pAl values are still lower than those of the aluminium chelators in clinical use but are high enough to be studied deeper for other applications.

- The stability of the complexes with bivalent metal ions decreases as the length of the linker increases. This is due to the involvement of the nitrogen atoms in the linker in copper and zinc coordination. Based on the found values of stability constants, only ligand A1 could find some application as copper chelator in clinical settings, and as copper and zinc chelator in environmental remediation.

Conflict of interest

All the authors state that there is no conflict of interest.

Acknowledgements

VMN and RB acknowledge the financial support by MIUR-PRIN 2015 - 2015MP34H3_002. VMN and CC thank Fondazione Banco di Sardegna and Regione Autonoma della Sardegna (Progetti Biennali di Ateneo Annualità 2016).

Appendix A. Supplementary data

Supplementary material related to this article can be found, in the online version, at doi:https://doi.org/10.1016/j.jtemb.2018.04.010.

References

[1] R. Galanello, R. Origa, Review: beta-thalassemia, Orphanet J. Rare Dis. 21 (2010) 5–11.
[2] C. Hershko, A.M. Konijn, G. Link, Iron chelators for thalassaemia, Br. J. Haematol. 101 (3) (1998) 399–406.
[3] Y. Ma, T. Zhou, X. Kong, R.C. Hider, Chelating agents for the treatment of systemic iron overload, Curr. Med. Chem. 19 (17) (2012) 2816–2827.
[4] J.L. Kwiatkowski, Current recommendations for chelation for transfusion-dependent thalassemia, Ann. N.Y. Acad. Sci. 1368 (1) (2016) 107–114.
[5] D. Rund, Thalassemia 2016: modern medicine battles an ancient disease, Am. J. Hematol. 91 (1) (2016) 15–21.
[6] A.N. Saliba, A.R. Harb, A.T. Taher, Iron chelation therapy in transfusion-dependent thalassemia patients: current strategies and future directions, J. Blood Med. 6 (2015) 197–209.
[7] E.A. Roberts, M.L. Schilsky, Diagnosis and treatment of Wilson disease: an update, Hepatology 47 (6) (2008) 2089–2111.
[8] D. Leštan, C.-l. Luo, X.-d. Li, The use of chelating agents in the remediation of metal-contaminated soils: a review, Environ. Pollut. 153 (1) (2008) 3–13.
[9] G. Chauhan, K. Pant, K. Nigam, Chelation technology: a promising green approach for resource management and waste minimization, Environ. Sci.: Processes Impacts 17 (1) (2015) 12–40.
[10] A. Serrano, F. Pinto-Ibieta, A. Braga, D. Jeison, R. Borja, F. Fermoso, Risks of using EDTA as an agent for trace metals dosing in anaerobic digestion of olive mill solid waste, Environ. Technol. 38 (24) (2017) 3137–3144.
[11] G. DalCorso, A. Manara, S. Piasentin, A. Furini, Nutrient metal elements in plants, Metallomics 6 (10) (2014) 1770–1788.
[12] E. Bloem, S. Haneklaus, R. Haensch, E. Schnug, EDTA application on agricultural soils affects microelement uptake of plants, Sci. Total Environ. 577 (2017) 166–173.
[13] G. Tóth, T. Hermann, M. Da Silva, L. Montanarella, Heavy metals in agricultural soils of the European Union with implications for food safety, Environ. Int. 88 (2016) 299–309.
[14] V.M. Nurchi, G. Crisponi, J.I. Lachowicz, S. Murgia, T. Pivetta, M. Remelli, A. Rescigno, J. Niclós-Gutíerrez, J.M. González-Pérez, A. Domínguez-Martín, Iron (III) and aluminum (III) complexes with hydroxypyrone ligands aimed to design kojic acid derivatives with new perspectives, J. Inorg. Biochem. 104 (5) (2010) 560–569.
[15] V.M. Nurchi, J.I. Lachowicz, G. Crisponi, S. Murgia, M. Arca, A. Pintus, P. Gans, J. Niclos-Gutierrez, A. Domínguez-Martín, A. Castineiras, M. Remelli, Z. Szewczuk, T. Lis, Kojic acid derivatives as powerful chelators for iron (III) and aluminium (III), Dalton Trans. 40 (22) (2011) 5984–5998.
[16] L. Toso, G. Crisponi, V.M. Nurchi, M. Crespo-Alonso, J.I. Lachowicz, M.A. Santos, S.M. Marques, J. Niclós-Gutiérrez, J.M. González-Pérez, A. Domínguez-Martín, D. Choquesillo-Lazarte, Z. Szewczuk, A family of hydroxypyrone ligands designed and synthesized as iron chelators, J. Inorg. Biochem. 127 (2013) 220–231.
[17] V.M. Nurchi, G. Crisponi, M. Arca, M. Crespo-Alonso, J.I. Lachowicz, M.A. Zoroddu, M. Peana, G. Pichiri, M.A. Santos, S.M. Marques, J. Niclos-Gutierrez, M.J. Gonzalez-Perez, A. Dominguez-Martin, D. Choquesillo-Lazarte, Z. Szewczuk, D. Mansoori, L. Toso, A new bis-3-hydroxy-4-pyrone as a potential therapeutic iron chelating agent. Effect of connecting and side chains on the complex structures and metal ion selectivity, J. Inorg. Biochem. 141 (2014) 132–143.
[18] L. Toso, G. Crisponi, V.M. Nurchi, M. Crespo-Alonso, J.I. Lachowicz, D. Mansoori, M. Arca, M.A. Santos, S.M. Marques, L. Gano, J. Niclós-Gutíerrez, J.M. González-Pérez, A. Domínguez-Martín, D. Choquesillo-Lazarte, Z. Szewczuk, Searching for new aluminium chelating agents: a family of hydroxypyrone ligands, J. Inorg. Biochem. 130 (2014) 112–121.
[19] J.I. Lachowicz, V.M. Nurchi, G. Crisponi, Md.G.J. Pelaez, A. Rescigno, P. Stefanowicz, M. Cal, Z. Szewczuk, Metal coordination and tyrosinase inhibition studies with Kojic-βAla-Kojic, J. Inorg. Biochem. 151 (2015) 36–43.
[20] M. Peana, S. Medici, V.M. Nurchi, J.I. Lachowicz, G. Crisponi, M. Crespo-Alonso, M.A. Santos, M.A. Zoroddu, An NMR study on the 6, 6′-(2-(diethylamino) ethylazanediyl) bis (methylene) bis (5-hydroxy-2-hydroxymethyl-4H-pyran-4-one) interaction with Al III and Zn II ions, J. Inorg. Biochem. 148 (2015) 69–77.
[21] J. Lachowicz, V. Nurchi, G. Crisponi, M. Jaraquemada-Pelaez, M. Arca, A. Pintus, M. Santos, C. Quintanova, L. Gano, Z. Szewczuk, Hydroxypyridinones with enhanced iron chelating properties. Synthesis, characterization and in vivo tests of 5-hydroxy-2-(hydroxymethyl) pyridine-4 (1 H)-one, Dalton Trans. 45 (15) (2016) 6517–6528.
[22] M. Peana, S. Medici, V.M. Nurchi, J.I. Lachowicz, G. Crisponi, E. Garribba, D. Sanna, M.A. Zoroddu, Interaction of a chelating agent, 5-hydroxy-2-(hydroxymethyl) pyridin-4 (1H)-one, with Al (III), Cu (II) and Zn (II) ions, J. Inorg. Biochem. 171 (2017) 18–28.
[23] A. Albert, E.P. Serjeant, Ionization Constants of Acids and bases: a Laboratory Manual, Methuen (1962).
[24] E. Farkas, É.A. Enyedy, H. Csóka, A comparison between the chelating properties of some dihydroxamic acids, desferrioxamine B and acetohydroxamic acid, Polycyclic Aromatic Compounds 18 (18) (1999) 2391–2398.
[25] http://www.hyperquad.co.uk/HQ2013.htm, (2016).
[26] www.hyperquad.co.uk/HypSpec2014.htm.

[27] O.V. Dolomanov, L.J. Bourhis, R.J. Gildea, J.A. Howard, H. Puschmann, OLEX2: a complete structure solution, refinement and analysis program, J. Appl. Crystallogr. 42 (2) (2009) 339–341.
[28] G.M. Sheldrick, Crystal structure refinement with SHELXL, Acta Crystallographica Section C: Structural Chemistry 71 (1) (2015) 3–8.
[29] G.M. Sheldrick, SHELXT–Integrated space-group and crystal-structure determination, Acta Crystallographica Section A: Foundations Adv. 71 (1) (2015) 3–8.
[30] V.M. Nurchi, T. Pivetta, J.I. Lachowicz, G. Crisponi, Effect of substituents on complex stability aimed at designing new iron (III) and aluminum (III) chelators, J. Inorg. Biochem. 103 (2) (2009) 227–236.
[31] D.P. da Costa, S.M. Nobre, B.G. Lisboa, Jd.M. Vicenti, D.F. Back, 2, 2′-Dihydroxy-N, N′-(ethane-1, 2-diyl) dibenzamide, Acta Crystallogr. Sect. E Struct. Rep. Online 69 (2) (2013) o201-o201.
[32] A. De Robertis, C. Foti, O. Giuffrè, S. Sammartano, Dependence on ionic strength of polyamine protonation in NaCl aqueous solution, J. Chem. Eng. Data 46 (6) (2001) 1425–1435.
[33] C. De Stefano, O. Giuffrè, S. Sammartano, Protonation constants of ethylenediamine, diethylenetriamine, and spermine in NaCl (aq), NaI (aq),(CH3) 4NCl (aq), and (C2H5) 4NI (aq) at different ionic strengths and t= 25 °C, J. Chem. Eng. Data 50 (6) (2005) 1917–1923.
[34] S. Cascio, A. De Robertis, C. Foti, Protonation of diamines H2N−(CH2) n− NH2 (n= 2− 10) in NaCl aqueous solution at different ionic strengths, J. Chem. Eng. Data 44 (4) (1999) 735–738.
[35] E.J. Enemark, T. Stack, Spectral and structural characterization of two ferric coordination modes of a simple bis (catecholamide) ligand: metal-assisted self-assembly in a siderophore analog, Inorg. Chem. 35 (10) (1996) 2719–2720.
[36] P.J. Cappillino, P.C. Tarves, G.T. Rowe, A.J. Lewis, M. Harvey, C. Rogge, A. Stassinopoulos, W. Lo, W.H. Armstrong, J.P. Caradonna, Synthesis and characterization of a family of binuclear non-heme iron monooxygenase model compounds: evidence for a “phenolate/amide carbonyl (PAC) shift” upon oxidation, Inorg. Chim. Acta 362 (7) (2009) 2136–2150.
[37] C. Baes Jr, R. Mesmer, The hydrolysis of cations, in: R.E. Krieger (Ed.), Malabar, Wiley, New York, 1986, p. 1976.
[38] A. Agren, The complex formation between iron (III) ion and some phenols. IV. The acidity constant of the phenolic group, Acta Chem. Scand. 9 (1) (1955).
[39] V.M. Nurchi, G. Crisponi, J.I. Lachowicz, S. Medici, M. Peana, M.A. Zoroddu, Chemical features of in use and in progress chelators for iron overload, J. Trace Elem. Med Biol. 38 (2016) 10–18.
[40] E. Furia, R. Porto, 2-Hydroxybenzamide as a ligand. Complex formation with dioxouranium (VI), aluminum (III), neodymium (III), and nickel (II) ions, J. Chem. Eng. Data 53 (12) (2008) 2739–2745.
[41] M.A. Santos, S. Gama, L. Gano, G. Cantinho, E. Farkas, A new bis (3-hydroxy-4-pyridinone)-IDA derivative as a potential therapeutic chelating agent, Synthesis, Metal-Complexation Biological Assays, Dalton Transactions (21) (2004) 3772–3781.
[42] M. Eckshtain-Levi, R. Lavi, D. Yufit, M. Orio, R. Wanke, L. Benisvy, A novel dicompartmental bis-(2-hydroxyisophtalamide) macrocyclic ligand and its mononuclear Cu (II) and Ni (II) complexes, Dalton Trans. 41 (40) (2012) 12457–12467.
[43] A.I. Nguyen, R.G. Hadt, E.I. Solomon, T.D. Tilley, Efficient C–H bond activations via O 2 cleavage by a dianionic cobalt (ii) complex, Chem. Sci. 5 (7) (2014) 2874–2878.
[44] K. Maxcy, M. Turnbull, A redetermination of bis (ethylenediamine-N, N’) bis (perchlorato-O) copper (II), Acta Crystallogr. Sect. C Cryst. Struct. Commun. 55 (12) (1999) 1986–1988.
[45] A. Gasowska, L. Lomozik, R. Jastrzab, Mixed-ligand complexes of copper (II) ions with AMP and CMP in the systems with polyamines and non-covalent interaction between bioligands, J. Inorg. Biochem. 78 (2) (2000) 139–147.